Polyhedron 52 (2013) 196–206

Contents lists available at SciVerse ScienceDirect

Polyhedron

journal homepage: www.elsevier.com/locate/poly

Mn/Ce clusters from the use of pivalate and chelate ligands: $Mn^{III}_8Ce^{IV}$, $Mn^{III}_2Ce^{IV}_2$, and $Mn^{III}_4Ce^{III}_2$ products

Constantina Papatriantafyllopoulou [1], Khalil A. Abboud, George Christou *

Department of Chemistry, University of Florida, Gainesville, FL 32611-7200, USA

ARTICLE INFO

Article history:
Available online 10 October 2012

Dedicated to Alfred Werner, the father of coordination chemistry, on the 100th anniversary of his Nobel Prize in Chemistry in 1913.

Keywords:
Manganese(III) clusters
Cerium clusters
3d–4f clusters
Magnetochemistry
Pivalates

ABSTRACT

The reaction system $Mn^{II}/Ce^{III/IV}/(CH_3)_3CCO_2^-$ has been investigated and has yielded four Mn_xCe_y and one Mn^{III}_4 compounds. Reactions in the presence of $NBu^n_4MnO_4$ afforded a $Mn^{III}_8Ce^{IV}$ compound $[Mn_8CeO_8(Bu^tCO_2)_{12}(DMF)_4]$ (**1**), consisting of a Ce^{IV} atom inside a loop of eight Mn^{III} ions. Reactions also containing 1,10-phenanthroline (phen) or 2,2′-bipyridine (bpy) gave $[Mn_2Ce_2O_2(OH)_2(Bu^tCO_2)_4(NO_3)_4(phen)_2]$ (**2**) or $[Mn_2Ce_2O_2(OH)_2(Bu^tCO_2)_4(NO_3)_4(bpy)_2]$ (**3**), respectively, containing the $Mn^{III}_2Ce^{IV}_2O_2$ core. In contrast, reactions in the presence of 2-(hydroxymethyl)pyridine (hmpH) yielded the $Mn^{III}_4Ce^{III}_2$ cluster $[Mn_4Ce_2O_2(Bu^tCO_2)_5(NO_3)_5(hmp)_4]$ (**4**), with an unprecedented $[Mn_4Ce_2(\mu_4\text{-}O)_2]$ core, and a homometallic, butterfly-like Mn^{III}_4 cluster $[Mn_4O_2(Bu^tCO_2)_6(pic)_2(H_2O)_2]$ (**5**), in which oxidation of hmp^- to picolinate (pic^-) has occurred. Variable-temperature, dc and ac measurements were performed on polycrystalline samples of **1**–**5**. Fitting of the obtained magnetization (M) versus field (H) and temperature (T) data by matrix diagonalization, and including only axial anisotropy (zero-field splitting, ZFS), gave a ground state spin of $S = 5$ for **1**·2DMF. The magnetic susceptibility data for **2**·$2Et_2O$ and **3** up to 300 K were fit and revealed very weak ferromagnetic interactions between the Mn^{III} ions; $J = +0.5(2)\ cm^{-1}$ for **2**·$2Et_2O$, and $J = +0.3(1)\ cm^{-1}$ for **3**. Complexes **4**·3MeCN and **5**·$2Bu^tCO_2H$ have $S = 0$ ground states.

1. Introduction

Alfred Werner would no doubt be very pleasantly surprised by the enormous impact that coordination chemistry has had on a wide range of areas of modern chemistry and related disciplines. He would also no doubt be extremely proud that the basic principles of metal coordination number and geometry that he elucidated, and for which he was awarded the 1913 Nobel Prize in Chemistry, are the foundation for essentially all these studies. Our own work heavily relies on such 'Wernerian' principles, especially our interests in the fields of bioinorganic chemistry and molecular nanoscience. In bioinorganic chemistry, there is a continuing search for high oxidation state, oxide-bridged Mn coordination clusters to model the Mn_4CaO_5 unit that is the oxygen-evolving complex (OEC) near photosystem II (PSII) [1]. Other main group metals and the lanthanides can replace the Ca^{2+} *in vitro*, thus providing valuable tools for gaining insights into the nature and mechanism of action of the OEC [2]. In the materials science arena, certain 3d metal coordination clusters possess unusual magnetic properties and can function as nanoscale magnets, i.e., single-molecule magnets (SMMs) [3]. SMMs are discrete molecules that behave as superparamagnets, exhibiting slow magnetization relaxation at low temperatures and thus displaying magnetization hysteresis analogous to that observed in bulk magnets. SMMs thus represent a molecular approach to nanomagnetism, and they have been proposed for several technological applications [4]. The magnetic behavior of SMMs results from the combination of a large ground spin state (S) with a large and negative (easy-axis) magnetoanisotropy (D). Most trivalent lanthanide ions possess large single-ion anisotropy, and this was the stimulus for the initial interest in 3d/4f cluster chemistry as an alternative approach for the synthesis of SMMs [5]. With Mn, a large number of Mn/4f clusters are now known, including, $Mn_{12}Dy_6$ [6], $Mn_{21}Ln$ [7], Mn_6Ln_2 [8], $Mn_{12}Gd$ [9], $Mn_{11}Gd_2$ [10a], Mn_5Ln_4 [10b], and Mn_9Dy_8 [10c] examples.

A sub-class of the large family of Mn/4f clusters are the Mn/Ce heterometallic compounds [11]. Although Ce^{IV} is diamagnetic, these compounds are nevertheless of interest for various reasons: (1) Ce and mixed Mn/Ce oxides have been extensively used in heterogeneous catalytic oxidation processes, including sub- and super-critical catalytic wet oxidations for the treatment of wastewater containing toxic organic and inorganic pollutants such as ammonia, acetic acid, pyridine, phenol, polyethylene–glycol, and others [12]; (2) the Ce^{IV} ion favors formation of oxide-bridged species containing Mn^{III} and/or Mn^{IV}, and has been employed for the synthesis of many Mn/Ce compounds with interesting magnetic

* Corresponding author. Tel.: +1 352 392 8314; fax: +1 352 392 8757.
E-mail address: christou@chem.ufl.edu (G. Christou).
[1] Present address: Department of Chemistry, University of Cyprus, Nicosia, Cyprus.

0277-5387/$ - see front matter © 2012 Elsevier Ltd. All rights reserved.
http://dx.doi.org/10.1016/j.poly.2012.09.052

properties, such as a Mn_8Ce SMM with $S = 16$ [11a,b]; and (3) small nuclearity Mn/Ce^{IV} clusters are amenable to fitting of variable-temperature magnetic susceptibility data to yield the magnitudes of the various Mn...Mn intramolecular exchange interactions, which in turn allows a deeper understanding of the magnetic properties of other Mn/4f species containing anisotropic 4f ions for which spin–orbit coupling effects preclude accurate magnetic susceptibility fits [13].

As part of our continuing interest in Mn/Ce chemistry, we have been seeking to develop synthetic procedures to new Mn/Ce compounds. In the present work, we have investigated the use of pivalate ($Bu^tCO_2^-$) as the carboxylate, and the effect on the identity of the obtained products of the presence of *N*,*N*′-chelates such as 1,10-phenanthroline (phen) and 2,2′-bipyridine (bpy), or the *N*,*O*-chelating/bridging anion of 2-(hydroxymethyl)pyridine. *N*,*N*′-chelates are known to stabilize high oxidation species [14], whereas hmp^- groups often support ferromagnetic coupling between metal atoms, and have thus yielded many polynuclear 3d and 4f metal clusters with large *S* values and SMM properties [15], but few mixed 3d/4f compounds [16,17]. The employment of these groups in Mn/Ce cluster chemistry was thus expected to yield compounds with new structural features, and this has turned out to be the case. The syntheses, crystal structures and magnetic properties of the obtained compounds are discussed in this work, spanning a homometallic Mn^{III}_4 cluster, two $Mn^{III}_2Ce^{IV}_2$ species, a $Mn^{III}_4Ce^{III}_2$ cluster, and a $Mn^{III}_8Ce^{IV}$ cluster, some of which possess unprecedented structural features in Mn/Ce chemistry.

2. Experimental

2.1. General and physical measurements

All manipulations were performed under aerobic conditions using reagents and solvents as received. $NBu^n_4MnO_4$ was synthesized as described elsewhere [18]. *WARNING:* Permanganate (MnO_4^-) salts are potentially explosive; such compounds should be synthesized and used in small quantities, and treated with utmost care at all times.

Microanalyses (C, H, N) were performed by the in-house facilities of the Chemistry Department at the University of Florida. IR spectra (4000–400 cm^{-1}) were recorded on a Nicolet Nexus 670 spectrometer with the samples prepared as KBr pellets. Variable-temperature dc and ac magnetic susceptibility data were collected using a Quantum Design MPMS-XL SQUID magnetometer equipped with a 7 T magnet and operating in the 1.8–300 K range. The samples were embedded in solid eicosane to prevent torquing. Pascal's constants [19] were used to estimate the diamagnetic corrections, which were subtracted from the experimental susceptibilities to give the molar paramagnetic susceptibilities (χ_M).

2.2. Compound preparation

2.2.1. $[Mn_8CeO_8(Bu^tCO_2)_{12}(DMF)_4]$ (**1**)

A stirred colorless solution of Bu^tCO_2H (1.88 mL, 16.4 mmol) in hot DMF (30 mL) was treated with $Mn(O_2CMe)_2{\cdot}4H_2O$ (0.36 g, 1.5 mmol) and $Ce(NO_3)_3{\cdot}6H_2O$ (0.65 g, 1.5 mmol). The solution was stirred for 10 min, during which time solid $NBu^n_4MnO_4$ (0.18 g, 0.50 mmol) was added in three portions. The resulting dark brown slurry was filtered and the filtrate left to stand undisturbed in a closed flask. After 2 days, X-ray quality dark red prismatic crystals of **1**·2DMF had grown and were collected by filtration, washed with cold Me_2CO (2 × 3 mL) and dried under vacuum. Yield, 65%. The dried solid analyzed satisfactorily as **1**·2DMF. *Anal.* Calc. for $C_{78}H_{150}CeMn_8N_6O_{38}$: C, 39.70; H, 6.41; N, 3.56. Found: C, 39.32; H, 6.29; N, 3.40%. IR (KBr, cm^{-1}): 2961m, 2929m, 2913w, 1653s, 1584s, 1542s, 1484s, 1457w, 1423s, 1377m, 1228s, 1110m, 1030w, 937w, 787m, 695m, 678m, 614s, 571s, 511m, 451m.

2.2.2. $[Mn_2Ce_2O_2(OH)_2(Bu^tCO_2)_4(NO_3)_4(phen)_2]$ (**2**)

A stirred colorless solution of Bu^tCO_2H (1.88 mL, 16.4 mmol) in hot MeCN (30 mL) was treated with $Mn(O_2CMe)_2{\cdot}4H_2O$ (0.24 g, 1.0 mmol) and $Ce(NO_3)_3{\cdot}6H_2O$ (0.43 g, 1.0 mmol). The solution was stirred for 10 min, during which time solid $NBu^n_4MnO_4$ (0.18 g, 0.50 mmol) was added in three portions. The resulting dark brown slurry was filtered and the filtrate was treated with phen (0.18 g, 1.0 mmol) The solution was stirred at room temperature for a further 10 min, filtered, and the filtrate layered with Et_2O (60 mL). After 3 days, X-ray quality dark red crystals of **2**·2Et_2O had grown and were collected by filtration, washed with cold Et_2O (2 × 3 mL) and dried under vacuum. Yield, 60%. The dried solid analyzed satisfactorily as solvent-free **2**. *Anal.* Calc. for $C_{44}H_{54}Ce_2Mn_2N_8O_{24}$: C, 35.93; H, 3.70; N, 7.62. Found: C, 36.02; H, 3.53; N, 7.49%. IR (KBr, cm^{-1}): 3394m, 2976m, 2928m, 2870w, 1734w, 1624w, 1581m, 1495s, 1484s, 1461s, 1415m, 1351m, 1312m, 1280s, 1223s, 1146m, 1106m, 1028m, 895w, 868m, 856m, 812m, 787m, 727s, 651s, 634s, 592s, 517m, 500m, 433w, 414w.

2.2.3. $[Mn_2Ce_2O_2(OH)_2(Bu^tCO_2)_4(NO_3)_4(bpy)_2]$ (**3**)

This complex was prepared in the same manner as complex **2** but using bpy (0.16 g, 1.0 mmol) in place of phen. After 3 days, dark-red prismatic crystals were collected by filtration, washed with Et_2O (2 × 5 mL), and dried under vacuum. Yield, 60%. The dried solid analyzed satisfactorily as **3**. *Anal.* Calc. for $C_{40}H_{54}Ce_2Mn_2N_8O_{24}$: C, 33.77; H, 3.83; N, 7.88. Found: C, 33.77; H, 3.67; N, 7.71%. IR (KBr, cm^{-1}): 3395m, 2946m, 2932m, 2874w, 1621w, 1580m, 1495s, 1482s, 1460s, 1417m, 1356m, 1309m, 1280s, 1223s, 1148m, 1106m, 1029m, 892w, 868m, 861m, 819m, 787m, 726s, 649s, 635s, 588s, 514m, 503m, 425w.

2.2.4. $[Mn_4Ce_2O_2(Bu^tCO_2)_5(NO_3)_5(hmp)_4]$ (**4**)

A stirred colorless solution of Bu^tCO_2H (1.88 mL, 16.4 mmol) in hot MeCN (30 mL) was treated with $Mn(O_2CMe)_2{\cdot}4H_2O$ (0.24 g, 1.0 mmol) and $(NH_4)_2[Ce(NO_3)_6]$ (0.55 g, 1.0 mmol), which caused a rapid color change to dark red. The resulting solution was treated with hmpH (0.19 mL 1.0 mmol) and stirred at room temperature for a further 10 min. Then it was filtered and the filtrate left undisturbed in an open flask. Slow evaporation of the solvent at room temperature gave dark red crystals of **4**·3MeCN, which were kept in mother liquor for X-ray analysis, and dried under vacuum for other solid-state studies. Yield, 75%. The dried solid analyzed as **4**·2MeCN. *Anal.* Calc. for $C_{53}H_{75}Ce_2Mn_4N_{11}O_{31}$: C, 34.18; H, 4.06; N, 8.27. Found: C, 34.68; H, 4.17; N, 7.93%. IR (KBr, cm^{-1}): 2968m, 2934m, 2879w, 1600m, 1480m, 1380s, 1314m, 1305w, 1223s, 1109w, 1055s, 892w, 774m, 662, 540m.

2.2.5. $[Mn_4O_2(Bu^tCO_2)_6(pic)_2(H_2O)_2]$ (**5**)

A stirred colorless solution of Bu^tCO_2H (1.88 mL, 16.4 mmol) in hot MeCN (30 mL) was treated with $Mn(O_2CMe)_2{\cdot}4H_2O$ (0.24 g, 1.0 mmol) and $(NH_4)_2[Ce(NO_3)_6]$ (1.65 g, 3.0 mmol), which caused a rapid color change to dark red. The resulting solution was treated with hmpH (0.19 mL 1.0 mmol) and stirred at room temperature for a further 10 min. Then it was filtered, and the filtrate left undisturbed in an open flask. Slow evaporation of the solvent at room temperature gave dark red crystals, which were kept in mother liquor for X-ray analysis, and dried under vacuum for other solid-state studies. Yield: ~55% based on Mn. The dried solid analyzed as **5**·2$Bu^tCO_2H{\cdot}5H_2O{\cdot}2$MeCN. *Anal.* Calc. for $C_{56}H_{86}Mn_4N_4O_{29}$: C, 44.39; H, 6.79; N, 3.70. Found: C, 44.21; H, 6.49; N, 3.60%. IR (KBr, cm^{-1}): 3392m, 2960m, 2931m, 2872w, 1701m, 1624w, 1588m, 1554m, 1481m, 1409s, 1356s, 1297m, 1224s, 1183s,

1049m, 1027m, 890w, 845w, 773m, 712m, 697w, 653s, 609s, 462m.

2.3. Single-crystal X-ray crystallography

For **1**·2DMF, data were collected at 173 K on a Siemens SMART PLATFORM equipped with a CCD area detector and a graphite monochromator utilizing Mo Kα radiation (λ = 0.71073 Å). Cell parameters were refined using 8192 reflections. A full sphere of data (1850 frames) was collected using the ω-scan method (0.3° frame width). The first 50 frames were re-measured at the end of data collection to monitor instrument and crystal stability (maximum correction on I was < 1%). For **2**·2Et_2O, **4**·3MeCN and **5**·2Bu^tCO_2H, data were collected at 100 K on a Bruker DUO system equipped with an APEX II area detector and a graphite monochromator utilizing Mo Kα radiation. Cell parameters were refined using 9999 reflections. Data were collected using the ω-scan method (0.5° frame-width). Absorption corrections by integration were applied based on measured indexed crystal faces. The structures were solved by direct methods in SHELXTL6 [20], and refined on F^2 using full-matrix least squares. Non-H atoms were treated anisotropically, whereas H atoms were calculated in ideal positions and refined as riding on the respective C atoms. Unit cell parameters and structure solution and refinement data are listed in Table 1.

For **1**·2DMF, the asymmetric unit consists of four Mn_8Ce clusters and eight DMF solvent molecules. The latter were disordered and could not be modeled properly, thus program SQUEEZE [21], a part of the PLATON package of crystallographic software, was used to calculate the solvent disorder area and remove its contribution to the overall intensity data. Two of the clusters have disordered t-butyl groups: two in Ce1A and three in Ce1D. A total of 4340 parameters were refined in the final cycle of refinement using 52 572 reflections with $I > 2\sigma(I)$ to yield R_1 and wR_2 of 3.94% and 10.37%, respectively.

For **2**·2Et_2O, the asymmetric unit consists of a half Mn_2Ce_2 cluster and one Et_2O molecule in a general position. A total of 406 parameters were refined in the final cycle of refinement using 7095 reflections with $I > 2\sigma(I)$ to yield R_1 and wR_2 of 2.42% and 6.33%, respectively.

For **4**·3MeCN, the asymmetric unit consists of a half Mn_4Ce_2 cluster located on an inversion center and 1.5 MeCN solvent molecules. The O14/O15 ligand position has a disorder between a $Bu^tCO_2^-$ ion and a NO_3^- ion. Atoms C3–C5 are also disordered and were refined with their occupation factors fixed at 0.5 because of symmetry. The occupation factors of the Bu^tCO_2/NO_3^- disordered ligands are also fixed at 0.5 because of symmetry. A total of 460 parameters were refined in the final cycle of refinement using 7014 reflections with $I > 2\sigma(I)$ to yield R_1 and wR_2 of 2.93% and 5.61%, respectively.

For **5**·2Bu^tCO_2H, the asymmetric unit consists of a half Mn_4 cluster and a Bu^tCO_2H molecule. The H atoms on the bound H_2O and Bu^tCO_2H were obtained from a difference Fourier map and refined without constraint. There were 425 parameters in the final cycle of refinement using 6627 reflections with $I > 2\sigma(I)$ to yield R_1 and wR_2 of 2.43% and 6.15%, respectively.

3. Results and discussion

3.1. Synthesis

Many reaction systems under a variety of conditions were explored, differing in reagent ratios, solvents, crystallization methods, etc., before the procedures described below were developed. The reaction in DMF of $Mn(O_2CMe)_2$, $Ce(NO_3)_3$ and $NBu^n_4MnO_4$ in a 3:3:1 molar ratio in the presence of an excess of Bu^tCO_2H under heating yielded a dark brown solution from which $[Mn_8CeO_8(Bu^tCO_2)_{12}(DMF)_4]$ (**1**) was subsequently isolated. The reaction involves oxidation by the MnO_4^- of the Mn^{II} and some Ce^{III} to give the $Mn^{III}_8Ce^{IV}$ product. This is summarized in Eq. (1); the excess of Ce^{III} is not included.

$$6Mn^{II} + 2Ce^{III} + 2Mn^{VII} \rightarrow Mn^{III}_8Ce^{IV} + Ce^{IV} \quad (1)$$

The effect of *N,N′*-chelates L (L = phen or bpy) on the above reaction was then explored, at different reagent ratios. The reaction in MeCN of $Mn(O_2CMe)_2$, $Ce(NO_3)_3$, L and $NBu^n_4MnO_4$ in a 2:2:2:1

Table 1
Crystallographic data for complexes **1**·2DMF, **2**·2Et_2O, **4**·3MeCN and **5**·2Bu^tCO_2H.

	1	**2**	**4**	**5**
Formula[a]	$C_{78}H_{150}CeMn_8N_6O_{38}$	$C_{52}H_{72}Ce_2Mn_2N_8O_{26}$	$C_{55}H_{78}Ce_2Mn_4N_{12}O_{31}$	$C_{52}H_{84}Mn_4N_2O_{24}$
M (g mol^{-1})[a]	2359.68	1615.30	1903.29	1342.98
Crystal system	triclinic	triclinic	triclinic	monoclinic
Space group	$P\bar{1}$	$P\bar{1}$	$P\bar{1}$	$P2_1/c$
a (Å)	25.260(4)	9.8815(8)	11.3383(12)	12.8187(4)
b (Å)	27.805(4)	12.7697(10)	13.4599(14)	12.0101(4)
c (Å)	32.004(4)	13.8057(11)	14.689(2)	21.3493(6)
α (°)	82.553(2)	93.616(1)	111.409(2)	90
β (°)	88.578(2)	91.256(1)	105.938(2)	93.354(2)
γ (°)	82.963(2)	104.903(1)	99.648(2)	90
V (Å^3)	22 120(5)	1678.8(2)	1914.8(4)	3281.18(18)
Z	8	1	1	4
T (K)	173(2)	100(2)	100(2)	100(2)
λ (Å)[b]	0.71073	0.71073	0.71073	0.71073
ρ_{calc} (g cm^{-3})	1.417	1.598	1.651	1.359
μ (mm^{-1})	1.360	1.780	1.891	0.826
Measured/independent	164 716/68 973	23 179/7706	33 685/8787	35 415/7554
R_{int}	0.0387	0.0284	0.0566	0.0250
Obsd [$I > 2\sigma(I)$]	52 572	7095	7014	6627
R_1[c]	0.0394	0.0242	0.0293	0.0243
wR_2[d]	0.1037	0.0633	0.0561	0.0615
Goodness-of-fit (GOF) on F^2	1.105	1.034	0.931	1.016
$(\Delta\rho)_{max,min}$ (e Å^{-3})	0.976, −1.234	1.512, −0.906	1.064, −0.695	0.392, −0.223

[a] Including solvent molecules.
[b] Mo Kα radiation.
[c] $R_1 = \Sigma(|F_o| - |F_c|)/\Sigma(|F_o|)$ for observed reflections.
[d] $wR_2 = \{\Sigma[w(F_o^2 - F_c^2)^2]/\Sigma[w(F_o^2)^2]\}^{1/2}$.

ratio in the presence of an excess of Bu^tCO_2H under heating yielded a dark brown solution from which was isolated $[Mn_2Ce_2O_2(OH)_2(Bu^tCO_2)_4(NO_3)_4L_2]$ (L = phen, **2**; L = bpy, **3**). The redox reaction is summarized in Eq. (2).

$$2Mn^{II} + 2Ce^{III} + Mn^{VII} \rightarrow Mn^{III}{}_2Ce^{IV}{}_2 + Mn^{III} \quad (2)$$

Small changes to the reaction conditions to **1**–**3** (reagent ratios, crystallization methods, and the presence of added anions) had no influence on the identity of the isolated products.

We then employed hmpH in the reaction system to explore how its bridging ability might affect the identity of the product. The reaction in MeCN between $Mn(O_2CMe)_2$, $(NH_4)_2[Ce(NO_3)_6]$ and hmpH in a 1:1:1 ratio in the presence of an excess of Bu^tCO_2H under heating gave a dark red solution from which was isolated $[Mn_4Ce_2O_2(Bu^tCO_2)_5(NO_3)_5(hmp)_4]$ (**4**). The same procedure but with a 1:3:1 ratio gave instead $[Mn_4O_2(Bu^tCO_2)_6(pic)_2(H_2O)_2]$ (**5**). In both these reactions, the only oxidizing agent is Ce^{IV}, and the redox reactions to **4** and **5** are summarized in Eqs. (3) and (4). In Eq. (4), the large excess of Ce^{IV} in the reaction rationalizes

$$4Mn^{II} + 4Ce^{IV} \rightarrow Mn^{III}{}_4Ce^{III}{}_2 + 2Ce^{III} \quad (3)$$

$$4Mn^{II} + 12Ce^{IV} \rightarrow Mn^{III}{}_4 + 4Ce^{III} + 8Ce^{IV} \quad (4)$$

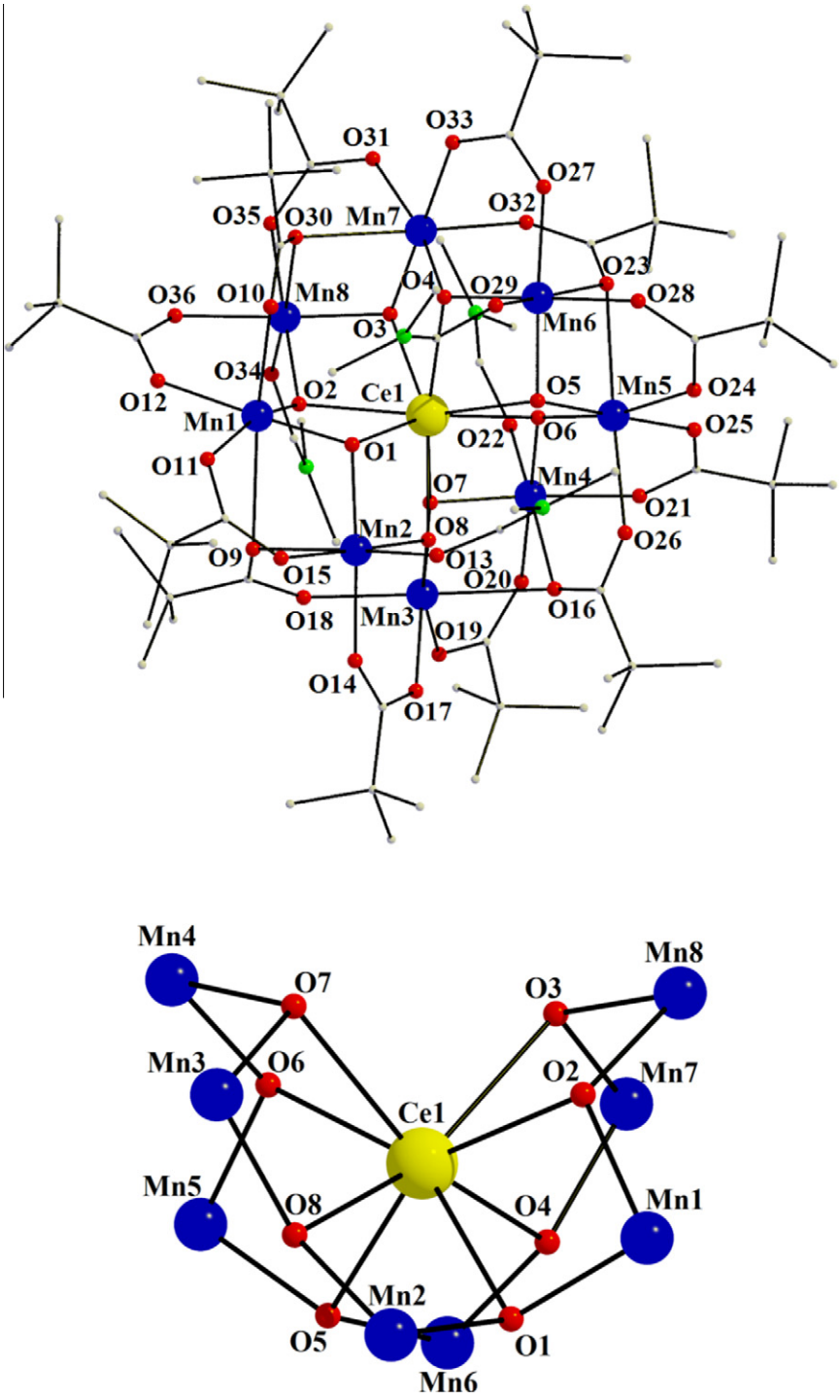

Fig. 1. The molecular structure of **1** (top) and its core (bottom). H atoms have been omitted for clarity.

the subsequent observation in the crystal structure (*vide infra*) that the chelate groups are 2-picolinate (pic$^-$), and these were obviously formed from oxidation of hmpH groups. Analogous oxidation of hmpH to picH has been previously reported [22]. The reaction solvent does not affect the identity of the obtained products, **4** and **5** also being obtained from MeOH, DMF, and $MeNO_2$; however, the yields were lower and the solids contaminated with other products.

3.2. Description of structures

Labeled plots of the complete structure and the core of $[Mn_8CeO_8(Bu^tCO_2)_{12}(DMF)_4]$ (**1**) are shown in Fig. 1. Selected interatomic distances and angles are listed in Table 2. Complex **1**·2DMF contains four independent Mn_8Ce molecules (**1a**–**1d**) whose bond lengths and angles differ only marginally; thus, only the structure of **1a** will be discussed. The cluster contains one Ce^{IV} and eight Mn^{III} ions bridged by eight μ_3-O^{2-} and 12 $Bu^tCO_2^-$ groups. The structure can be described as a central Ce^{IV} ion held within a non-planar, saddle-like $[Mn^{III}_8(\mu_3\text{-}O)_8]^{8+}$ loop by the triply-bridging oxide ions (Fig. 1, bottom). Atoms Mn2, Mn4, Mn6 and Mn8 form an almost perfect tetrahedron (e.g., Mn2–Ce1–Mn6 is 111.26°), whereas the remaining four Mn atoms form a distorted (flattened) tetrahedron (e.g., Mn3–Ce1–Mn5 is 91.88°). Within this description, the Ce^{IV} ion occupies the center of both Mn_4 tetrahedra.

Peripheral ligation around the $[Mn_8CeO_8]^{12+}$ core is provided by eight *syn*, *syn* doubly- and four triply-bridging $Bu^tCO_2^-$ groups. There are four DMF terminal ligands (O13, O22, O29, O34) on Mn^{III} atoms Mn2, Mn4, Mn6 and Mn8. The Ce atom is eight-coordinate with distorted dodecahedral geometry, and the Ce–O bond lengths (2.32–2.41 Å) are typical for eight-coordinate Ce^{IV} [23b]. All the Mn atoms are six-coordinate with near octahedral geometry and display Jahn–Teller (JT) elongation axis, as expected for high spin Mn^{III} ions, with the JT bonds being at least 0.1–0.2 Å larger than the other Mn^{III}–O bonds. The eight JT axes are not parallel but essentially randomly oriented (Fig. S1 of Supporting Information). The metal oxidation states are consistent with the metric parameters, and were confirmed by bond valence sum (BVS) calculations (Table S1) [23]. Complex **1** is a new addition to the small family of Mn_8Ce clusters with different carboxylates [11b], being the first with pivalate groups.

Table 2
Selected interatomic distances (Å) and angles (°) for **1**·2DMF.

Mn1–O1	1.851(3)	Mn5–O5	1.874(2)
Mn1–O2	1.868(2)	Mn5–O6	1.867(2)
Mn2–O1	1.886(2	Mn6–O4	1.852(2)
Mn2–O8	1.857(2)	Mn6–O5	1.887(2)
Mn3–O7	1.875(2)	Mn7–O3	1.870(2)
Mn3–O8	1.863(2)	Mn7–O4	1.863(2)
Mn4–O6	1.861(2)	Mn8–O2	1.853(3)
Mn4–O7	1.890(2)	Mn8–O3	1.883(3)
Ce1–O1	2.409(2)	Ce1–O5	2.387(2)
Ce1–O2	2.327(3)	Ce1–O6	2.320(2)
Ce1–O3	2.394(2)	Ce1–O7	2.410(2)
Ce1–O4	2.332(2)	Ce1–O8	2.320(2)
Ce1···Mn1	3.3332(7)	Ce1···Mn5	3.3156(7)
Ce1···Mn2	3.3650(6)	Ce1···Mn6	3.3647(6)
Ce1···Mn3	3.3349(7)	Ce1···Mn7	3.3308(7)
Ce1···Mn4	3.3756(7)	Ce1···Mn8	3.3591(7)
Mn1···Mn2	3.0356(10)	Mn1···Mn8	3.2434(8)
Mn2···Mn3	3.2382(9)	Mn5···Mn6	3.0120(8)
Mn3···Mn4	3.0134(8)	Mn6···Mn7	3.2472(8)
Mn4···Mn5	3.2519(8)	Mn7···Mn8	3.0114(9)
Ce1–O1–Mn1	102.18(11)	Ce1–O5–Mn5	101.51(10)
Ce1–O1–Mn2	102.48(10)	Ce1–O5–Mn6	103.23(10)
Ce1–O2–Mn1	104.69(12)	Ce1–O6–Mn4	107.17(10)
Ce1–O2–Mn8	106.37(11)	Ce1–O6–Mn5	104.21(10)
Ce1–O3–Mn7	102.03(11)	Ce1–O7–Mn3	101.49(10)
Ce1–O3–Mn8	102.86(10)	Ce1–O7–Mn4	102.77(10)
Ce1–O4–Mn6	106.5(1)	Ce1–O8–Mn2	106.83(11)
Ce1–O4–Mn7	104.58(10)	Ce1–O8–Mn3	105.24(11)

Labeled plots of the complete structure and core of $[Mn_2Ce_2O_2(OH)_2(Bu^tCO_2)_4(NO_3)_4(phen)_2]$ (**2**) are shown in Fig. 2. Selected interatomic distances and angles are listed in Table 3. The cluster contains a $[Mn^{III}_2Ce^{IV}_2(\mu_3\text{-}O)_2]^{10+}$ core consisting of a Mn_2Ce_2 parallelogram with each Mn_2Ce triangular unit bridged by a μ_3-O^{2-} ion (O3). The core is additionally bridged at two of its edges (Mn1Ce1′ and its symmetry equivalent) by a μ-OH^- group (O12), and at each of its four edges by a μ-$Bu^tCO_2^-$ group. Since only two of its edges are mono-atomically bridged, the core is somewhat different from the defective dicubane unit that is relatively common in both homo- and hetero-metallic cluster chemistry [11i,17,24,25].

Two chelating phen groups complete distorted octahedral geometry at the Mn^{III} atoms, and four chelating NO_3^- groups complete nine-coordination at the Ce^{IV} atoms. The metal oxidation states and the protonation level of OH^- and O^{2-} ions were confirmed by BVS calculations, which gave 2.98 for Mn, 3.92 for Ce, 1.91 for O^{2-}, and 0.99 for OH^-. As expected, the Mn^{III} atoms are JT elongated, with Mn1–N2 [2.248(2) Å] and Mn1–O4 [2.143(2) Å] distinctly longer than the other bonds [1.864(1)–2.071(2) Å]. The JT axes are aligned parallel as a result of the symmetry of the molecule. The molecular packing reveals intermolecular O–H···O hydrogen-bonds between μ-OH^- groups (O12) on one molecule and NO_3^- ligands (O10) on an adjacent molecule [O12···O10′ = 2.830(2) Å]. This leads to a 1-D chain parallel to the *ac* plane (Fig. S2). We are unaware of another compound containing a $Mn^{III}_2Ce^{IV}_2$ core as in **2**, although complexes with the $Mn^{III}_2Ce^{III}_2$ core are known [11i]. Complex **3** was concluded from the infra-red and elemental analysis data and unit-cell comparison to be isostructural with **2**, and its crystal structure was therefore not pursued. Given the similarity in structures, it probably also exhibits intermolecular O–H···O hydrogen-bonds.

Labeled plots of the complete structure and core of $[Mn_4Ce_2O_2(Bu^tCO_2)_5(NO_3)_5(hmp)_4]$ (**4**) are shown in Fig. 3, and selected interatomic distances and angles are listed in Table 4. The structure consists of four Mn^{III} and two Ce^{III} atoms bridged by two μ_4-O^{2-}, four η^1:η^2:μ-hmp^-, one η^2:η^2:μ_3-$Bu^tCO_2^-$, one η^2:η^2:μ_3-NO_3^-, and four η^1:η^1:μ-$Bu^tCO_2^-$ groups. Peripheral ligation is completed by two chelating NO_3^- groups on each nine-coordinate Ce^{III} atom. The $[Mn_4Ce_2(\mu_4\text{-}O^{2-})_2]$ central core can also be described as two oxide-centered Mn_2Ce triangular units with the central O^{2-} of one unit bridging to the Ce^{III} atom of the other. This $[Mn_4Ce_2(\mu_4\text{-}O^{2-})_2]$ topology has not been previously reported in Mn/Ce chemistry. Complex **4** is the second reported Mn_4Ce_2 cluster, but it is distinctly different from the previous example $[Mn_4Ce_2O_2(Me\text{-}sao)_6(NO_3)_4(O_2CMe)_2(H_2O)_2]$ (Me-sao^{2-} is the methylsalicyloximato ion); the latter contains four Mn^{IV} atoms instead of four Mn^{III} atoms as in **4**, and a core topology comprising two Mn_2Ce triangular units linked by η^2:η^2:μ_4 oximato groups [11f].

A partially labeled representation of centrosymmetric $[Mn_4O_2(Bu^tCO_2)_6(pic)_2(H_2O)_2]$ (**5**) is shown in Fig. 4. Selected interatomic distances and angles are listed in Table 5. The molecule is a new member of the family of Mn^{III}_4 'planar-butterfly' complexes containing a $[Mn_4(\mu_3\text{-}O^{2-})_2]^{8+}$ core and a Mn_4 rhombus topology [15a,25,26,29] including one previous example with pic$^-$ ligands and a centrosymmetric structure, namely $[Mn_4O_2(MeCO_2)_6(pic)_2(MeCN)_2]$ [26a]. Oxide atom O2 is 0.417 Å above and below the Mn_4 plane. The four sides of the Mn_4 core are additionally bridged alternately by one or two μ-$Bu^tCO_2^-$ groups. Distorted octahedral geometry at each Mn^{III} atom is completed by a chelating pic$^-$ on Mn2 and Mn2′, and a terminal H_2O on Mn1 and Mn1′. The Mn oxidation states and the O^{2-} nature of atom O2 were confirmed by Mn and O BVS calculations, which gave values of 2.94 (Mn1), 2.91

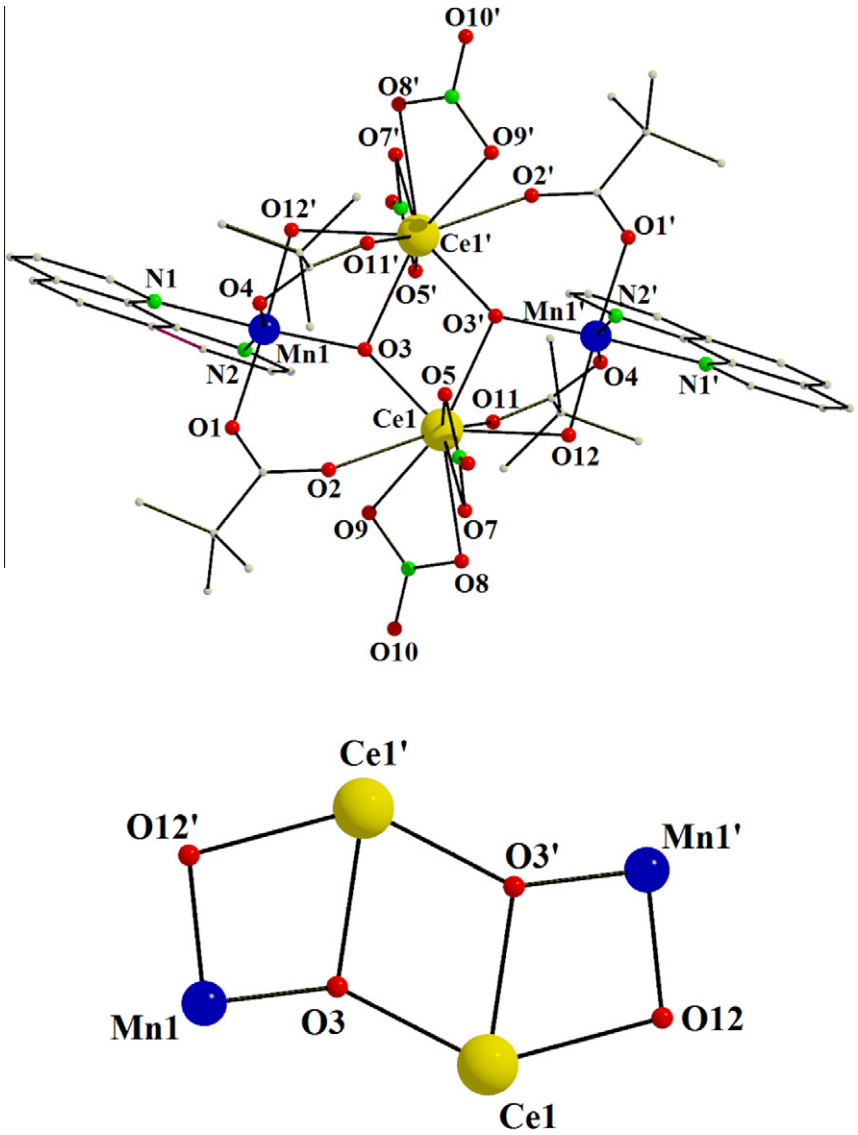

Fig. 2. The structure of **2** (top) and its core (bottom). H atoms have been omitted for clarity.

Table 3
Selected interatomic distances (Å) and angles (°) for **2**·2Et$_2$O.

Mn1–O1	1.932(2)	Ce1–O7	2.589(2)
Mn1–O3	1.864(1)	Ce1–O8	2.481(2)
Mn1–O4	2.143(2)	Ce1–O9	2.587(2)
Mn1–O12′[a]	1.905(2)	Ce1–O11	2.326(2)
Mn1–N1	2.077(2)	Ce1–O12	2.337(2)
Mn1–N2	2.248(2)	Mn1···Mn1′	6.059(2)
Ce1–O2	2.385(2)	Ce1···Ce1′	3.610(2)
Ce1–O3	2.147(1)	Mn1···Ce1	3.762(2)
Ce1–O3′	2.284(1)	Mn1···Ce1′	3.273(2)
Ce1–O5	2.447(2)		
O1–Mn1–O12′	177.0(1)	O5–Ce1–O7	50.7(1)
N1–Mn1–N2	77.1(1)	Ce1–O3–Mn1	139.4(1)
N1–Mn1–O3	170.6(1)	Ce1–O12–Mn1′	100.5(1)
O3–Ce1–O3′	70.9(1)	Ce1–O3–Ce1′	109.1(1)

[a] Symmetry code: (′) = 2 − *x*, 1 − *y*, −*z*.

(Mn2) and 1.89 (O2). As expected, the Mn^{III} atoms show JT distortions, consisting of elongations of the O1–Mn1–O5 and O3–Mn2–O7 axes [23]. The four JT axes divide into two symmetry-related pairs essentially perpendicular (90.6°) to each other (Fig. S3).

A packing diagram reveals extensive O–H···O hydrogen-bonding (Table 6) between lattice Bu^{t}CO$_2$H molecules (O11, O12) and either the uncoordinated O atoms of pic$^-$ ligands (O10) or the water ligands (O1), leading to the formation of a 2-D network in the *bc* plane (Fig. S4). There are also intramolecular hydrogen-bonds between the water ligands and O atoms (O6) of a bridging pivalate group.

3.3. Magnetochemistry

3.3.1. Magnetic susceptibility studies on **1**·2DMF

Variable-temperature magnetic susceptibility measurements were performed on a powdered polycrystalline sample of **1**·2DMF, restrained in eicosane to prevent torquing, in a 1 kG (0.1 T) magnetic field and in the 5.0–300 K temperature range. The obtained data are shown as a $\chi_M T$ versus T plot in Fig. 5. $\chi_M T$ increases with decreasing temperature from 24.98 cm^3 K mol^{-1} at 300 K to a maximum of 33.87 cm^3 K mol^{-1} at 50 K, and then rapidly decreases to 15.56 cm^3 K mol^{-1} at 5 K. The 300 K value is close to the spin-only (g = 2) value of 24.00 cm^3 mol^{-1} K for eight high-spin Mn^{III} non-interacting ions (Ce^{IV} is diamagnetic, f^0). The $\chi_M T$ versus T plot profile indicates that the dominant exchange interactions within the molecule are

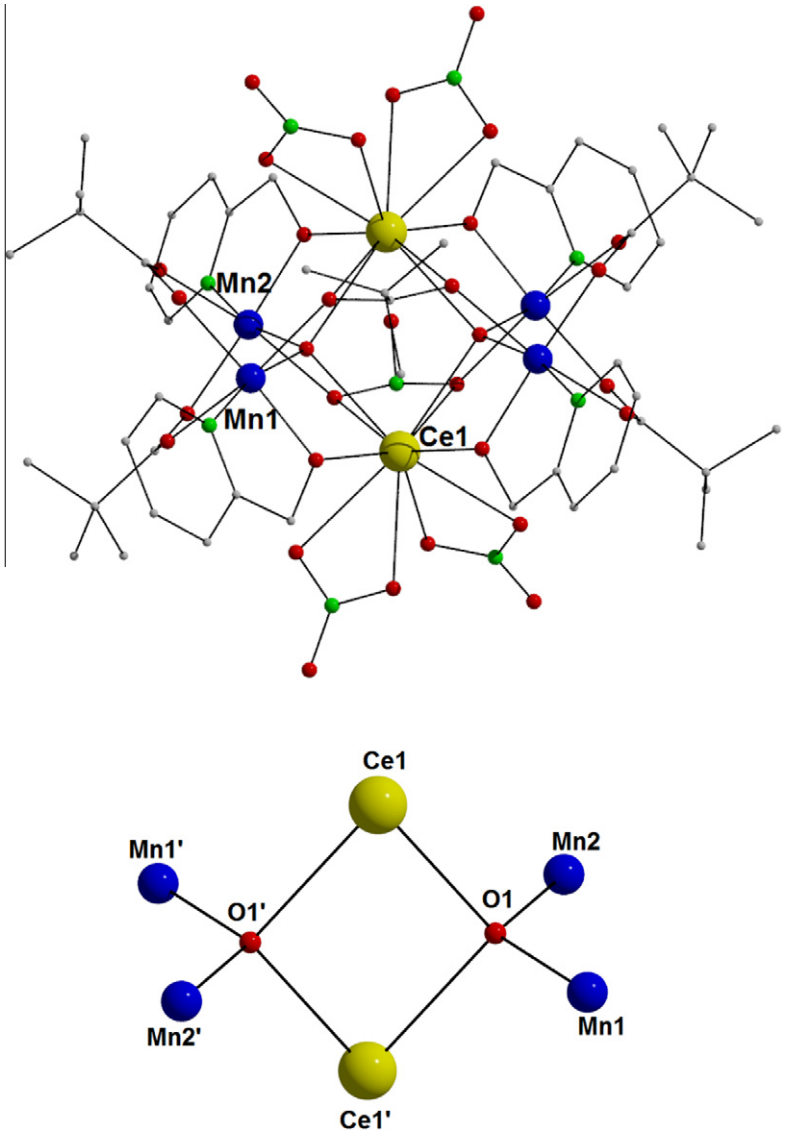

Fig. 3. The structure of **4** (top) and its core (bottom). H atoms have been omitted for clarity.

ferromagnetic, with weaker interactions (antiferro and/or ferromagnetic) assuming greater importance at lower temperatures.

In order to identify the ground state of **1**·2DMF, magnetization (M) data were collected in the 0.1–1.0 T field and 1.8–10 K temperature ranges. Attempts to fit the data were carried out using the program MAGNET [27] by diagonalization of the spin Hamiltonian matrix assuming only the ground state is populated, incorporating axial anisotropy ($D\hat{S}_z^2$) and Zeeman terms, and employing a full powder average. The corresponding spin Hamiltonian (H) is given by Eq. (5),

$$\mathcal{H} = D\hat{S}_z^2 + g\mu_B\mu_0\hat{S}\cdot H \qquad (5)$$

where D is the axial zero-field splitting (ZFS) parameter, $\hat{S}_z$ is the easy-axis spin operator, μ_0 is the vacuum permeability, and H is the applied field. The last term in Eq. (5) is the Zeeman energy associated with an applied magnetic field.

Preliminary efforts to fit all the data collected up to 1 T were unsuccessful, which was anticipated given the weak nature of many of the constituent pairwise exchange interactions in the $Mn^{III}_8Ce^{IV}$ family of clusters [11a,b]. This results in low-lying excited states, some of which will likely have greater S values than the ground state and thus approach or cross with the ground state in an applied field; this will lead to poor fits of the magnetization data because the fitting model assumes only the ground state is

Table 4
Selected interatomic distances (Å) and angles (°) for **4**.

Mn1–O1	1.9014(17)	Mn2–N2	2.039(2)
Mn1–O2	1.8740(18)	Ce1–O1	2.5101(17)
Mn1–O3	1.9291(18)	Ce1–O2	2.5326(17)
Mn1–O7	2.152(2)	Ce1–O8	2.614(2)
Mn1–O15′[a]	2.230(2)	Ce1–O9	2.5563(18)
Mn1–N1	2.044(2)	Ce1–O11	2.6442(19)
Mn2–O1	1.8814(19)	Ce1–O12	2.5948(18)
Mn2–O4	2.1354(18)	Ce1–O14	2.6671(19)
Mn2–O5	1.8920(18)	Ce1–O15	2.6518(18)
Mn2–O6	1.9359(19)	Ce1–O1′[a]	2.5622(18)
Mn2–O14	2.2884(18)	Ce1–O5′[a]	2.4685(19)
O1–Mn1–N1	167.69(9)	O1–Ce1–O12	162.92(5)
O2–Mn1–O3	171.75(8)	O2–Ce1–O12	131.31(6)
O7–Mn1–O15′[a]	172.62(7)	O8–Ce1–O9	49.62(6)
O5–Mn2–O6	172.60(8)	O11–Ce1–O12	48.80(6)
O1–Mn2–N2	165.89(8)	Mn1–O1–Mn2	115.02(9)
O4–Mn2–O14	172.28(7)	Ce1–O1–Ce1′[a]	104.66(6)

[a] Symmetry code: (′) = 1 − x, 2 − y, 1 − z.

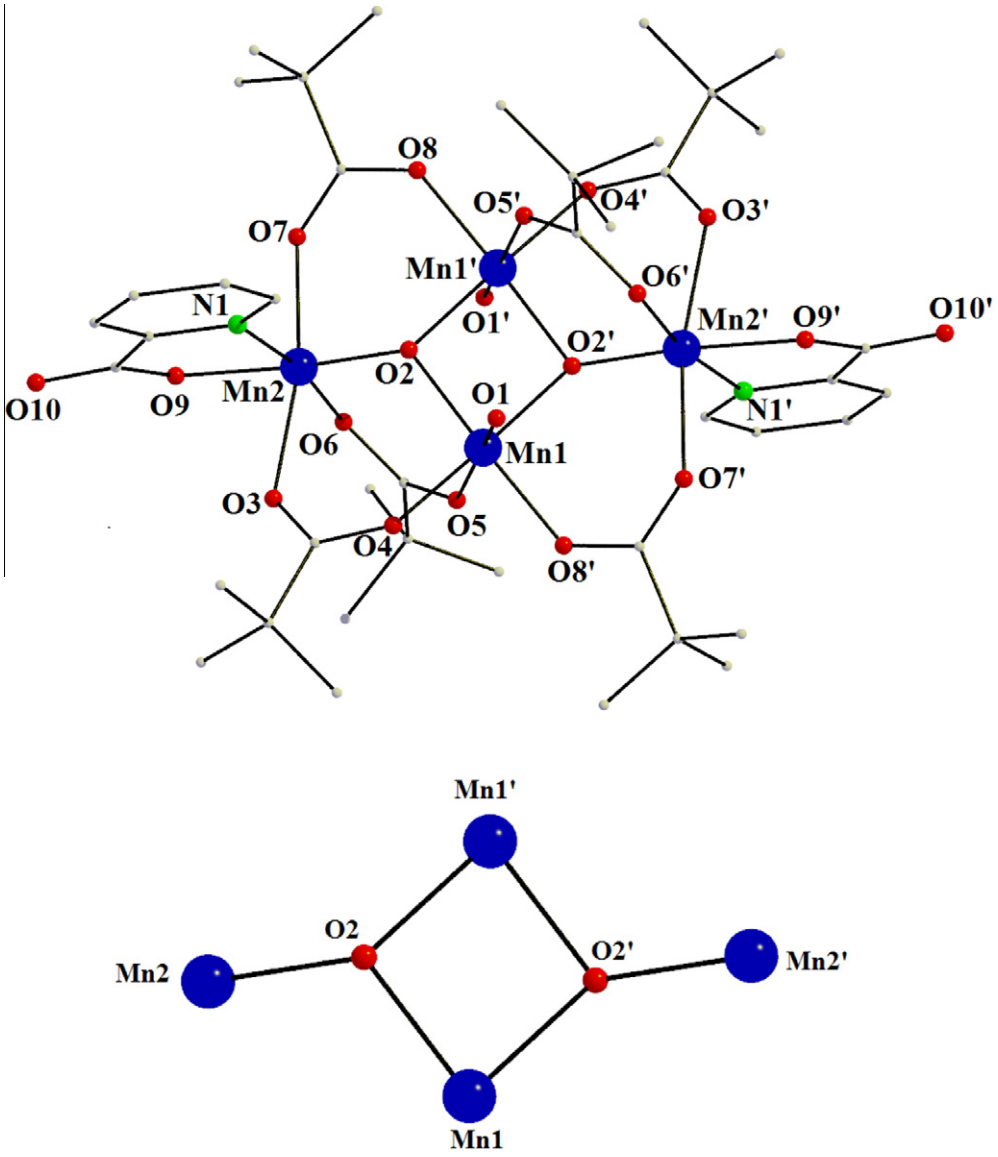

Fig. 4. The molecular structure of **5** (top) and its core (bottom). H atoms have been omitted for clarity.

Table 5
Selected interatomic distances (Å) and angles (°) for **5**·2Bu^{t}CO$_2$H.

Mn1–O1	2.322(2)	Mn2–O6	1.945(2)
Mn1–O2	1.897(2)	Mn2–O7	2.146(2)
Mn1–O2′[a]	1.911(2)	Mn2–O9	1.951(2)
Mn1–O4	1.950(2)	Mn2–N1	2.055(2)
Mn1–O5	2.152(2)	Mn1···Mn1′	2.892(2)
Mn1–O8′	1.928(2)	Mn2···Mn2′	5.954(2)
Mn2–O2	1.859(2)	Mn1···Mn2	3.266(2)
Mn2–O3	2.152(2)	Mn1···Mn2′	3.354(2)
O1–Mn1–O5	167.8(1)	O6–Mn2–N1	89.8(1)
O2–Mn1–O2′	81.1(1)	O9–Mn2–N1	80.5(1)
O2–Mn1–O8′	174.53(4)	Mn1–O2–Mn1′	98.9(1)
O2–Mn2–O9	170.3(1)	Mn1–O2–Mn2	120.7(2)
O3–Mn2–O7	168.2(1)	Mn1′–O2–Mn2	125.7(2)

[a] Symmetry code: (′) = 1 − *x*, 1 − *y*, 1 − *z*.

Table 6
Hydrogen-bonding interactions in the crystal structure of **5**·2Bu^{t}CO$_2$H.

Interaction	D···A (Å)	H···A (Å)	D–H···A (°)
O1–H1···O6	2.868(3)	2.34(1)	122.3(1)
O11–H11···O10[a]	2.627(3)	1.81(1)	164.7(1)
O1–H2···O12[a]	2.957(3)	2.16(1)	168.3(1)

A = acceptor atom; D = donor atom.
[a] O11 and O12 belong to Bu^{t}CO$_2$H molecules.

populated. To nevertheless try to estimate the ground state, we used only data collected at the weakest fields of 0.1–0.4 T to minimize field-induced problems from low-lying excited states [17], and these are shown as a reduced magnetization $M/N\mu_B$ versus H/T plot in Fig. 6, where N is Avogadro's number and μ_B is the Bohr magneton. The obtained fit with $S = 5$, $D = -0.60$ cm^{-1}, and $g = 1.97$ (solid line in Fig. 6) is only fair but indicates that the magnetization data are of the magnitude expected for an $S = 5$ ground state; the D value is merely an approximation given the quality of the fit.

An alternative probe of the ground state is provided by ac susceptibility studies, since they preclude any complications from a dc field. Thus, ac data on **1**·2DMF were collected in the 1.8–15 K range using a 3.5 G ac field oscillating in the 50–1000 Hz frequency range. The in-phase ac susceptibility (χ'_M) is shown as χ'_MT versus T in Fig. 7, and it can be seen to be rapidly decreasing with decreasing temperature, indicating depopulation of particularly low-lying

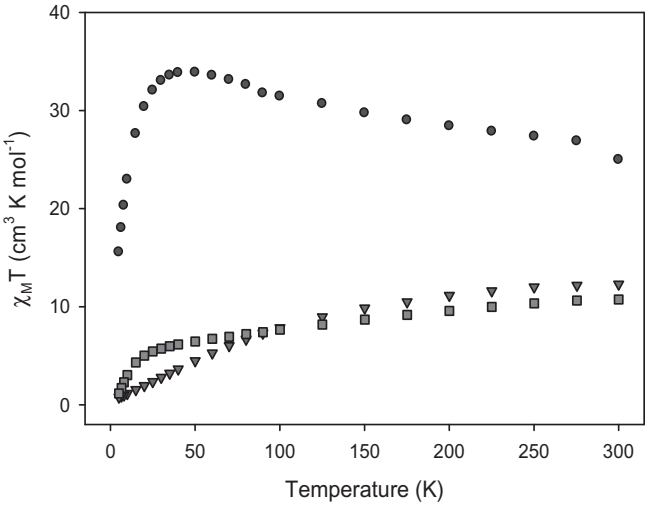

Fig. 5. $\chi_M T$ vs. T plots for **1**·2DMF (●), **4**·2MeCN (▼), and **5**·2Bu^{t}CO$_2$H (■) in a 0.1 T dc field.

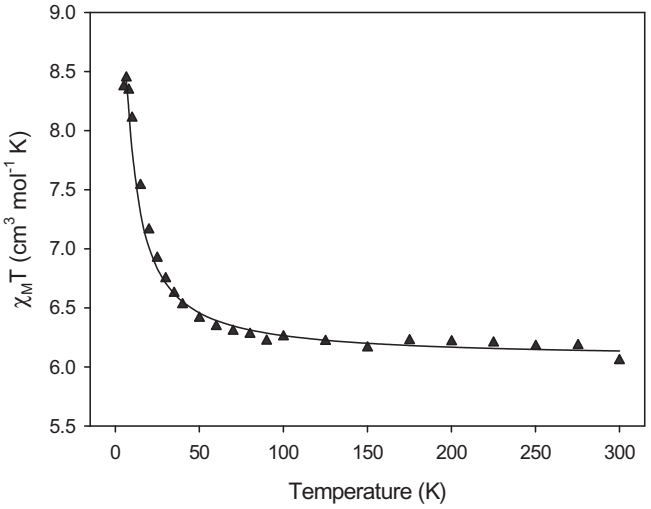

Fig. 8. $\chi_M T$ vs. T plot for **2** in a 0.1 T dc field. The solid line is the fit of the data to the theoretical expression; see the text for the fit parameters.

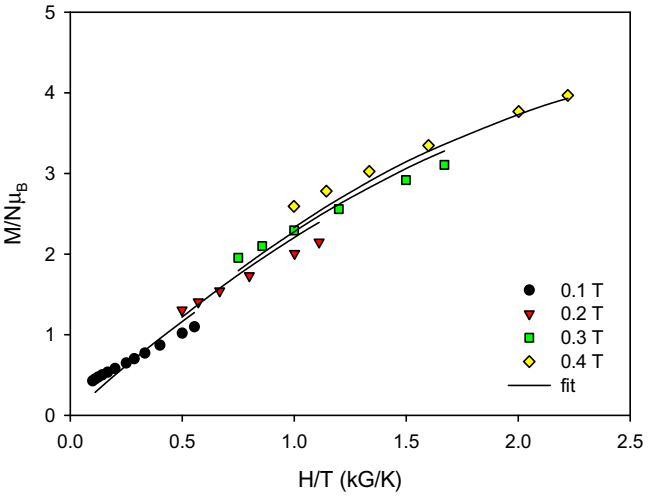

Fig. 6. Plot of reduced magnetization ($M/N\mu_B$) vs. H/T for complex **1**·2DMF at the indicated fields. The solid lines are the fit of the data for $S = 5$; see the text for the fit parameters.

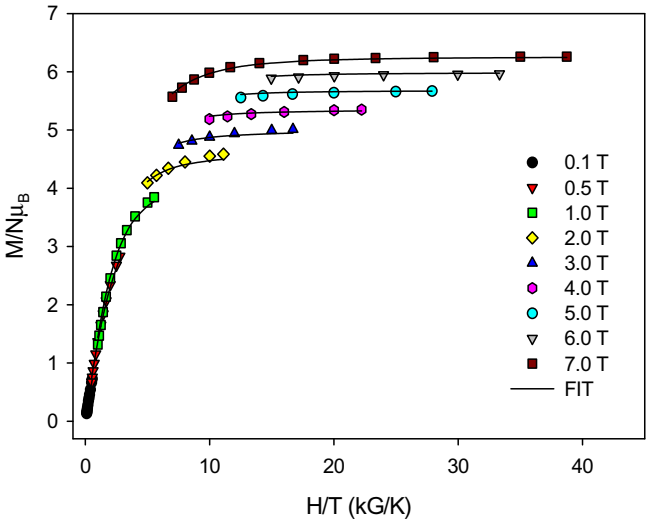

Fig. 9. Plot of reduced magnetization ($M/N\mu_B$) vs. H/T for complex **3** at the indicated fields. The solid lines are the fit of the data with $S = 4$; see the text for the fit parameters.

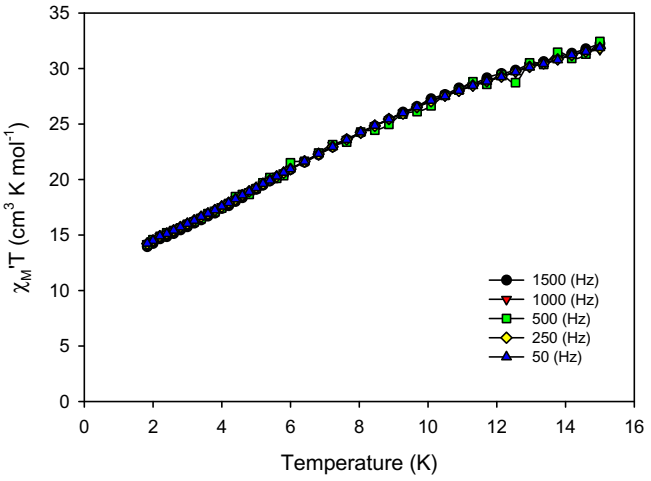

Fig. 7. In-phase ac susceptibility (χ'_M), plotted as $\chi'_M T$ vs. T, for **1**·2DMF in a 3.5 G field oscillating at the indicated frequencies.

excited states with S greater than the ground state; this is in agreement with the conclusions from the attempted fits of the dc magnetization data. The data extrapolate to ~12 cm^3 K mol^{-1} at 0 K, consistent with an $S = 5$ ground state with g slightly less than 2.0, as expected for a Mn^{III} cluster; the spin-only ($g = 2.0$) $\chi'_M T$ for $S = 4$, 5 and 6 are 10, 15 and 21 cm^3 K mol^{-1}, respectively. No frequency dependence of the $\chi'_M T$ signal is seen, suggesting **1**·2DMF is not a SMM, and the absence of an out-of-phase susceptibility (χ''_M) confirms this (Fig. S5).

The [Mn$_8$CeO$_8$(RCO$_2$)$_{12}$(solv)$_4$] (solv = H$_2$O, pyridine, MeCN or dioxane) family of clusters [11a,b] have previously been found to give a wide range of ground state S as a result of the many (often competing) constituent exchange parameters and small structural variations with the identity of R and solv. Ground states of $S = 4$ or 5 through $S = 16$ have been observed, the latter being the maximum possible and yielding an SMM. The $S = 5$ of the present **1**·2DMF is similar to the $S = 4$ or 5 determined for the [Mn$_8$CeO$_8$(MeCO$_2$)$_{12}$(py)$_4$] member.

*3.3.2. Magnetic susceptibility studies on **2** and **3***

Complexes **2** and **3** display similar magnetic data, as expected from their essentially identical structures. In both complexes, only the two Mn^{III} atoms are paramagnetic, since Ce^{IV} is diamagnetic. Given the four-bond separation between the Mn^{III} atoms, only very weak exchange coupling was anticipated. $\chi_M T$ for **2** is 6.06 $cm^3\,K\,mol^{-1}$ at 300 K, increases only slightly down to 100 K, and then increases more rapidly to 8.45 $cm^3\,K\,mol^{-1}$ at 5 K (Fig. 8). The $\chi_M T$ versus T profile indicates a very weak ferromagnetic interaction between the Mn^{III} ions. An analogous $\chi_M T$ versus T profile is seen for **3**, increasing from 6.08 $cm^3\,K\,mol^{-1}$ at 300 K to 7.85 $cm^3\,K\,mol^{-1}$ at 5 K (Fig. S6).

The isotropic Heisenberg spin Hamiltonian for a dinuclear complex such as **2** is given by Eq. (6), and its eigenvalues are given by Eq. (7), where J is the Mn^{III}–Mn^{III} exchange interaction,

$$\mathcal{H} = -2J\hat{S}_1 \cdot \hat{S}_2 \tag{6}$$

$$E(S_T) = -J[S_T(S_T+1)] \tag{7}$$

$S_1 = S_2 = 2$, S_T is the total spin of the molecule, and $E(S_T)$ is the energy of state S_T. Fitting of the experimental data for **2** to the corresponding Van Vleck equation [28] gave the solid line in Fig. 8, with fit parameters $J = +0.5(2)\,cm^{-1}$ and $g = 2.0(1)$, and a temperature-independent paramagnetism (TIP) term held constant at $100 \times 10^{-6}\,cm^3\,mol^{-1}$. The corresponding values for **3** were $J = +0.3(1)\,cm^{-1}$ and $g = 2.0(1)$. The $S_T = 3$ first excited state is at 4.0(1.6) and 2.4(0.8) cm^{-1} above the ground state for **2** and **3**, respectively.

In order to characterize the ground state further, magnetization data were collected for representative complex **3** in the 0.1–7.0 T and 1.8–10 K ranges (Fig. 9). The fit of the data (solid lines in Fig. 9) gave $S = 4$, $g = 1.85(5)$, and $D = -1.2(1)\,cm^{-1}$. The significant D value is consistent with the parallel alignment of the two Mn^{III} JT axes. The g value is slightly lower than might normally be expected for a Mn^{III} complex, but it reflects the fact that fits of magnetization data are not the most accurate way of obtaining g, and may also be partially due to the intermolecular interactions mediated through the hydrogen-bonds seen in the crystal structure of **2** (and, by implication, in **3**).

*3.3.3. Magnetic susceptibility studies on complex **4**·2MeCN*

The $\chi_M T$ for **4**·2MeCN steadily decreases with decreasing temperature from 12.29 $cm^3\,K\,mol^{-1}$ at 300 K to 0.78 $cm^3\,K\,mol^{-1}$ at 5.0 K (Fig. 5). The value at 300 K is very close to the spin-only ($g = 2.0$) value of 12.14 $cm^3\,K\,mol^{-1}$ expected for four Mn^{III} and two Ce^{III} ($^2F_{5/2}$ free ion, $S = {}^1/_2$, $L = 3$, $g_J = {}^6/_7$) non-interacting ions; this and the overall profile of the $\chi_M T$ versus T plot indicate the presence of weak antiferromagnetic interactions between the metal atoms, with the 5 K value indicating an essentially diamagnetic ground state. We also measured the ac susceptibility in the 1.8–15 K range (Fig. S4); the in-phase $\chi'_M T$ signal decreases steadily with decreasing temperature, heading for an essentially diamagnetic value of 0.2 $cm^3\,K\,mol^{-1}$. There was no out-of-phase χ''_M, indicating that **4** is not an SMM.

*3.3.4. Magnetic susceptibility studies on complex **5**·2Bu^{t}CO$_2$H*

The $\chi_M T$ for **5**·2Bu^{t}CO$_2$H steadily decreases with decreasing temperature from 10.74 $cm^3\,K\,mol^{-1}$ at 300 K to 6.46 $cm^3\,K\,mol^{-1}$ at 50 K, and then decreases more rapidly to 1.16 $cm^3\,mol^{-1}\,K$ at 5 K. The plot profile and the fact that it is clearly heading to ~0 $cm^3\,mol^{-1}\,K$ at 0 K indicate antiferromagnetic exchange interactions and a diamagnetic system at the lowest temperatures. Since previous studies on members of the Mn_4 family of butterfly complexes with the $[Mn_4(\mu_3\text{-}O^{2-})_2]^{8+}$ core have identified them as possessing an $S = 3$ ground arising from spin frustration effects [29], we interpret the low temperature diamagnetism for **5**·2Bu^{t}CO$_2$H as being due to intermolecular antiferromagnetic exchange interactions between $S = 3$ molecules propagated by the many intermolecular O–H···O hydrogen-bonds seen in the crystal structure. The same low temperature behavior was also seen in the ac susceptibility measurements in the 1.8–15 K range (Fig. S8); $\chi'_M T$ is heading for ~0 $cm^3\,mol^{-1}\,K$ at 0 K and there is no out-of-phase χ''_M signal down to 1.8 K.

4. Conclusions

One Mn_4 and four Mn/Ce clusters have been obtained from the reactions of Mn^{II} and Ce^{III} or Ce^{IV} sources with pivalate ions, in the presence or absence of phen, bpy, or hmpH. Cluster **1** is a new addition to the $Mn^{III}{}_8Ce^{IV}$ family, **2** and **3** possess a new $Mn^{III}{}_2Ce^{IV}{}_2$ core not previously seen in Mn/Ce chemistry, **4** also contains an unprecedented $Mn^{III}{}_4Ce^{III}{}_2$ core structure, and **5** is a new member of the $Mn^{III}{}_4$ 'butterfly' family. None of the complexes proved to be new SMMs, primarily due to the low ground state S values they were found to possess. Complexes **2** and **3** show a noticeable ferromagnetic interaction between the two Mn^{III} atoms despite the relatively large distance between the Mn atoms (6.06 Å).

Acknowledgements

This work was supported by NSF Grant DMR-1213030 and the Cyprus Research Promotion Foundation (Grant DIETHNIS/STO-XOS/0308/14).

Appendix A. Supplementary data

CCDC 876988, 876989, 876990 and 876991 contain the supplementary crystallographic data for **1**·DMF, **2**·2Et$_2$O, **4**·3MeCN and **5**·2ButCO$_2$H. These data can be obtained free of charge via http://www.ccdc.cam.ac.uk/conts/retrieving.html or from the Cambridge Crystallographic Data Centre, 12 Union Road, Cambridge CB2 1 EZ, UK; fax: (+44) 1223-336-033; or e-mail: deposit@ccdc.cam.ac.uk. Supplementary data associated with this article can be found, in the online version, at http://dx.doi.org/10.1016/j.poly.2012.09.052.

References

[1] (a) K.N. Ferreira, T.M. Iverson, K. Maghlaoui, J. Barber, S. Iwata, Science 303 (2004) 1831;
(b) Y. Umena, K. Kawakami, J.R. Shen, N. Kamiya, Nature 473 (2011) 55;
(c) S. Mukherjee, J.A. Stull, J. Yano, T.C. Stamatatos, K. Pringouri, T.A. Stich, K.A. Abboud, R.D. Britt, V.K. Yachandra, G. Christou, Proc. Nat. Acad. Sci. USA 109 (2012) 2257;
(d) J.S. Kanady, E.Y. Tsui, M.W. Day, T. Agapie, Science 333 (2011) 733.
[2] J.S. Vrettos, D.A. Stone, G.W. Brudvig, Biochemistry 40 (2001) 7937.
[3] (a) R. Bagai, G. Christou, Chem. Soc. Rev. 38 (4) (2009) 1011. and references cited therein;
(b) G. Christou, D. Gatteschi, D.N. Hendrickson, R. Sessoli, MRS Bull. 25 (2000) 66;
(c) D. Gatteschi, R. Sessoli, Angew. Chem., Int. Ed. 42 (2003) 268;
(d) G. Aromi, E.K. Brechin, Struct. Bonding (Berlin) 122 (2006) 1.
[4] (a) L. Bogani, W. Wernsdorfer, Nature Mater. 7 (2008) 179;
(b) M.N. Leuenberger, D. Loss, Nature 410 (2001) 789.
[5] S. Osa, T. Kido, N. Matsumoto, N. Re, A. Pochaba, J. Mrozinski, J. Am. Chem. Soc. 126 (2004) 420.
[6] J.-L. Liu, F.-S. Guo, Z.-S. Meng, Y.-Z. Zheng, J.-D. Leng, M.-L. Tong, L. Ungur, L.F. Chibotaru, K.J. Heroux, D.N. Hendrickson, Chem. Sci. 2 (2011) 1268.
[7] C. Papatriantafyllopoulou, W. Wernsdorfer, K.A. Abboud, G. Christou, Inorg. Chem. 50 (2011) 421.
[8] M. Holinska, D. Premuzic, I.-R. Jeon, W. Wernsdorfer, R. Clérac, S. Dehnen, Chem. Eur. J. 17 (2011) 9605.
[9] T.C. Stamatatos, S.J. Teat, W. Wernsdorfer, G. Christou, Angew. Chem., Int. Ed. 48 (2009) 521.
[10] (a) V. Mereacre, A.M. Ako, R. Clerac, W. Wernsdorfer, G. Filoti, J. Bartolome, C.E. Anson, A.K. Powell, J. Am. Chem. Soc. 129 (2007) 9248;
(b) V. Mereacre, A.M. Ako, R. Clerac, W. Wernsdorfer, I.J. Hewitt, C.E. Anson, A.K. Powell, Chem. Eur. J. 14 (2008) 3577;
(c) S. Langley, B. Moubaraki, K.S. Murray, Dalton Trans. 39 (2010) 5066.

[11] (a) A.J. Tasiopoulos, W. Wernsdorfer, B. Moulton, M.J. Zaworotko, G. Christou, J. Am. Chem. Soc. 125 (2003) 15274;
(b) A. Mishra, A.J. Tasiopoulos, W. Wernsdorfer, E.E. Moushi, B. Moulton, M.J. Zaworotko, K.A. Abboud, G. Christou, Inorg. Chem. 47 (2008) 4832;
(c) A.J. Tasiopoulos, T.A. O'Brien, K.A. Abboud, G. Christou, Angew. Chem., Int. Ed. 43 (2004) 345;
(d) A.J. Tasiopoulos, P.L. Milligan, K.A. Abboud, T.A. O'Brien, G. Christou, Inorg. Chem. 46 (2007) 9678;
(e) A. Mishra, A.J. Tasiopoulos, W. Wernsdorfer, K.A. Abboud, G. Christou, Inorg. Chem. 46 (2007) 3105;
(f) C.J. Milios, P.A. Wood, S. Parsons, D. Foguet-Albiol, C. Lampropoulos, G. Christou, S.P. Perlepes, E.K. Brechin, Inorg. Chim. Acta 360 (2007) 3932;
(g) M. Wang, D.-Q. Yuan, C.-B. Ma, M.-J. Yuan, M.-Q. Hu, N. Li, H. Chen, C.-N. Chen, Q.-T. Liu, Dalton Trans. 39 (2010) 7276;
(h) V. Mereacre, A.M. Ako, M.N. Akhtar, A. Lindemann, C.E. Anson, A.K. Powell, Helv. Chim. Acta 92 (2009) 2507;
(i) M.N. Akhtar, Y. Lan, V. Mereacre, R. Clérac, C.E. Anson, A.K. Powell, Polyhedron 28 (2009) 1698;
(j) G.V. Romanenko, E.Y. Fursova, V.I. Ovcharenko, Russ. Chem. Bull. Int. Ed. 58 (2009) 1.
[12] (a) H. Cao, S.L. Suib, J. Am. Chem. Soc. 116 (1994) 5334;
(b) M.I. Zaki, M.A. Hasan, L. Pasupulety, K. Kumary, New J. Chem. (1998) 875;
(c) Y.I. Matatov-Meytal, M. Sheintuch, Ind. Eng. Chem. Res. 37 (1998) 309;
(d) S. Hamoudi, K. Belkacemi, F. Larachi, Chem. Eng. Sci. 54 (1999) 3569;
(e) S. Hamoudi, K. Belkacemi, A. Sayari, F. Larachi, Chem. Eng. Sci. 56 (2001) 1275;
(f) Z.Y. Ding, M.A. Frisch, L. Li, E.F. Gloyna, Ind. Eng. Chem. Res. 35 (1996) 3257;
(g) G. Maayan, G. Christou, Inorg. Chem. 50 (2011) 7015.
[13] A. Panagiotopoulos, Th.F. Zafiropoulos, S.P. Perlepes, E. Bakalbassis, I. Masson-Ramade, O. Kahn, A. Terzis, C.P. Raptopoulou, Inorg. Chem. 34 (1995) 4918.
[14] S. Bhaduri, A.J. Tasiopoulos, M.A. Bolcar, K.A. Abboud, W.E. Streib, G. Christou, Inorg. Chem. 42 (2003) 1483.
[15] (a) J. Yoo, A. Yamaguchi, M. Nakano, J. Krzystek, W.E. Streib, L.-C. Brunel, H. Ishimoto, G. Christou, D.N. Hendrickson, Inorg. Chem. 40 (2001) 4604;
(b) E.C. Yang, D.N. Hendrickson, W. Wernsdorfer, M. Nakano, L.N. Zakharov, R.D. Sommer, A.L. Rheingold, M. Ledezma-Gairaud, G. Christou, J. Appl. Phys. 91 (2002) 7382;
(c) N.C. Harden, M.A. Bolcar, W. Wernsdorfer, K.A. Abboud, W.E. Streib, G. Christou, Inorg. Chem. 42 (2003) 7067;
(d) C.A. Christmas, J. Am. Chem. Soc. 115 (1993) 12483;
(e) T.C. Stamatatos, K.A. Abboud, W. Wernsdorfer, G. Christou, Angew. Chem., Int. Ed. 46 (2007) 884;
(f) T.C. Stamatatos, K.A. Abboud, W. Wernsdorfer, G. Christou, Angew. Chem., Int. Ed. 45 (2006) 4134;
(g) T.C. Stamatatos, K.A. Abboud, W. Wernsdorfer, G. Christou, Polyhedron 26 (2007) 2042;
(h) T.C. Stamatatos, K.M. Poole, K.A. Abboud, W. Wernsdorfer, T.A. O'Brien, G. Christou, Inorg. Chem. 47 (2008) 5006;
(i) M. Murugesu, S. Takahashi, A. Wilson, K.A. Abboud, W. Wernsdorfer, S. Hill, G. Christou, Inorg. Chem. 47 (2008) 4095;
(j) D.I. Alexandropoulos, S. Mukherjee, C. Papatriantafyllopoulou, C.P. Raptopoulou, V. Psycharis, V. Bekiari, G. Christou, T.C. Stamatatos, Inorg. Chem. 50 (2011) 11276.
[16] F. He, M.-L. Tong, Inorg. Chem. 44 (2005) 8285.
[17] C. Papatriantafyllopoulou, K.A. Abboud, G. Christou, Inorg. Chem. 50 (2011) 8959.
[18] J. B Vincent, H.R. Chang, K. Folting, J.C. Huffman, G. Christou, D.N. Hendrickson, J. Am. Chem. Soc. 109 (1987) 5703.
[19] R.C. Weast, CRC Handbook of Chemistry and Physics, CRC Press, Inc., Boca Raton, FL, 1984.
[20] SHELXTL6, Bruker-AXS, Madison, Wisconsin, USA, 2000.
[21] P. Van der Sluis, A.L. Spek, Acta Crystallogr., Sect. A 46 (1990) 194.
[22] E.C. Sanudo, E.K. Brechin, C. Boskovic, W. Wernsdorfer, J. Yoo, A. Yamaguchi, T.R. Concolino, K.A. Abboud, R.L. Rheingold, H. Ishimoto, D.N. Hendrickson, G. Christou, Polyhedron 22 (2003) 2267.
[23] (a) W. Liu, H.H. Thorp, Inorg. Chem. 32 (1993) 4102;
(b) P.L. Roulhac, G.J. Palenik, Inorg. Chem. 42 (2003) 118.
[24] (a) C. Benelli, M. Murrie, S. Parsons, R.E.P. Winpenny, J. Chem. Soc., Dalton Trans. (1999) 4125;
(b) A. Mishra, W. Wernsdorfer, S. Parsons, G. Christou, E.K. Brechin, Chem. Commun. (2005) 2086;
(c) M. Murugesu, A. Mishra, W. Wernsdorfer, K.A. Abboud, G. Christou, Polyhedron 25 (2006) 613;
(d) S. Mukherjee, M.R. Daniels, R. Bagai, K.A. Abboud, G. Christou, C. Lampropoulos, Polyhedron 29 (2010) 54.
[25] O. Roubeau, R. Clérac, Eur. J. Inorg. Chem. (2008) 4325. and references therein.
[26] (a) E. Libby, K. Folting, C.J. Huffman, J.C. Huffman, G. Christou, Inorg. Chem. 32 (1993) 2549;
(b) T. Taguchi, M.D. Daniels, K.A. Abboud, G. Christou, Inorg. Chem. 48 (2009) 9325;
(c) G. Christou, Acc. Chem. Res. 22 (1989) 328;
(d) E. Libby, J.K. McCusker, E.A. Schmitt, K. Folting, D.N. Hendrickson, G. Christou, Inorg. Chem. 30 (1991) 3486.
[27] E.R. Davidson, Magnet, Indiana University, Bloomington, IN, 1999.
[28] J.H. Van Vleck, The Theory of Electric and Magnetic Susceptibilities, Oxford Press, London, 1932.
[29] J.B. Vincent, C. Christmas, H.-R. Chang, Q. Li, P.D.W. Boyd, J.C. Huffman, D.N. Hendrickson, G. Christou, J. Am. Chem. Soc. 111 (1989) 2086.